Optics Letters

# Effective four-wave mixing in the lithium niobate on insulator microdisk by cascading quadratic processes

Shijie Liu,[1,2] Yuanlin Zheng,[1,2,6] Zhiwei Fang,[3,4] Xiaona Ye,[1,2] Ya Cheng,[3,4,5,7] and Xianfeng Chen[1,2]

[1]State Key Laboratory of Advanced Optical Communication Systems and Networks, School of Physics and Astronomy, Shanghai Jiao Tong University, Shanghai 200240, China
[2]Key Laboratory for Laser Plasma (Ministry of Education), Collaborative Innovation Center of IFSA, Shanghai Jiao Tong University, Shanghai 200240, China
[3]State Key Laboratory of Precision Spectroscopy, East China Normal University, Shanghai 200062, China
[4]XXL-The Extreme Optoelectromechanics Laboratory, School of Physics and Materials Science, East China Normal University, Shanghai 200241, China
[5]State Key Laboratory of High Field Laser Physics, Shanghai Institute of Optics and Fine Mechanics, Chinese Academy of Sciences, Shanghai 201800, China
[6]e-mail: ylzheng@sjtu.edu.cn
[7]e-mail: ya.cheng@siom.ac.cn

Received 28 January 2019; revised 20 February 2019; accepted 21 February 2019; posted 22 February 2019 (Doc. ID 358784); published 13 March 2019

**Whispering-gallery-mode resonators can dramatically enhance the light-matter interaction, benefitting nonlinear optics in many ways. Here, we demonstrate effective four-wave mixing (FWM) in a lithium niobate on insulator (LNOI) microdisk via cascaded quadratic nonlinear processes of second-harmonic generation and difference-frequency generation (i.e., cSHG/DFG) in the telecommunication band. The effective FWM process can be used as an optical parametric amplifier and can mimic an effectively strong Kerr nonlinearity. This shows the great promise of an integrated LNOI platform for nonlinear frequency conversion.** 

https://doi.org/10.1364/OL.44.001456

High-quality whispering-gallery-mode (WGM) microresonators have important applications in both fundamental physics and photonic applications due to their capability to dramatically boost the light-matter interaction [1]. They are a versatile platform for investigating nonlinear optical effects [2], as well as other important applications including low-threshold lasing [3], ultrasensitive sensing [4], optomechanics [5], and quantum optics [6]. Among many types of optical effects, quadratic nonlinearity in on-chip microresonators is of significance for the integration of frequency conversion, quantum sources, and frequency comb self-reference in both classical and nonclassical regimes. This has been intensively investigated utilizing crystalline materials lacking inversion symmetry, such as lithium niobate (LN) [7], gallium arsenide [8], and aluminum nitride [9], or at interfaces of centrosymmetric media like silica [10] and silicon nitride [11].

Lithium niobate (LN), which features a lot of favored optical properties such as a wide transmission window, relatively high refractive indices, large second-order susceptibility, and large piezoelectricity, is widely considered as an excellent basis for integrated nonlinear photonic functionalities. Recently, research regarding photonic integrated circuits (PICs) and on-chip microresonators on the novel lithium niobate on insulator (LNOI) platform has attracted remarkable attention [12,13]. Thanks to the developing LNOI and new fabrication technology, the propagation loss of light in LNOI waveguides has reached a record low level, and the $Q$ factor of LNOI microresonators has surpassed the order of $10^7$ [14,15]. Implementing nonlinearities using LNOI microresonators for nonlinear PICs is becoming advantageous and promising.

In LNOI microresonaotrs, quadratic nonlinear processes, such as second-harmonic generation (SHG) [16,17], sum-frequency generation (SFG) [18], parametric downconversion [19], and cascaded wave mixing [20,21], have been reported in different schemes to for various application demonstrations. Both modal phase matched SHG and difference frequency generation (DFG) processes have been demonstrated in the same LN microring resonator with a high conversion efficiency [22]. Furthermore, by harnessing the cascading of quadratic nonlinearity, it is feasible to achieve efficient third-order ones for nonlinear phase shift, and third- and high-order harmonic generation [20–25]. In many situations, the cascaded effect can outcompete a direct process. Thus, with the contemplated advances, there is more potential in LNOI microresonators for frequency conversion to be explored.

In this Letter, we report on the experimental realization of cascaded SHG and DFG (cSHG/DFG) to manifest an effective FWM based on second-order nonlinearity in a high-$Q$ LNOI

microdisk resonator. Through modal phase matching, efficient SHG in the visible range was observed with several-milliwatt input power at telecommunication wavelengths. By introducing a second input (acting as signal light) into the microdisk, idler light from cascaded DFG of the SH and the signal light, also via modal phase matching, is observed at the output. By utilizing cascaded quadratic nonlinearity, a large effective third-order nonlinearity can be obtained. Thus, the cascading process can achieve an efficient FWM process by simultaneously performing the two nonlinear processes in one quadratic microdisk.

The experimental setup is schematically depicted in Fig. 1. The fundamental wave (FW) from Laser1 and the signal light from Laser2 are launched from two external cavity tunable lasers (ECTLs) in the telecommunication C band wavelengths. The polarization of input is controlled by polarization controllers. A 2 × 2 50:50 single-mode fiber coupler is used to combine the two waves and launched into a tapered fiber on one path, and on the other path the input power is simultaneously monitored by a power meter. The tapered fiber, with a waist diameter of approximately 2 μm, is produced by the heating and pulling method. The LNOI microdisk sample is mounted on a precise 3D nanostage. The tapered fiber evanescently couples light into and out of the microdisk, in which nonlinear processes take place. The coupling efficiency is optimized by changing the input polarization and the contact point of the taper fiber and the microdisk (relating to the coupling loss). After the taper fiber-microcavity coupling system, the transmitted light is linked to another 2 × 2 90:10 fiber coupler. An optical spectrum analyzer (OSA) monitors the output spectrum from the 90% port of the fiber coupler, and the output from the 10% port is simultaneously monitored by an InGaAs photodetector and an oscilloscope. The LNOI microdisk is monitored by an optical microscope from a top view for both coupling optimization and SHG observation.

In our experiment, the microdisk was fabricated from commercial LNOI nanofilms (NANOLN Co.). The LN nanofilm is a *z*-cut single crystalline with a thickness of 300 nm, bonded on top of a 2-μm-thick silica layer, and the bottom substrate is bulk LN 0.5 mm thick. The LNOI microdisk microfabrication was performed at the Center for Advanced Electronic Materials and Devices (AEMD), Shanghai Jiao Tong University. The fabrication procedures include femtosecond laser micromachining, focused ion beam (FIB) milling, and high temperature annealing, which are the same with Refs. [26,27]. The diameter of the fabricated LNOI microdisk is 50 μm. The topography of the microdisk sample before hydrofluoric acid etching was analyzed by scanning electronic microscopy (SEM), as shown in Fig. 2(a). It can be seen that the FIB process can etch the edge of the microcavity with a high smoothness, which can achieve subnanometer rms precision. Figures 2(b) and 2(c) show the optical microscopic imaging of the scattered second harmonic (SH) during the SHG process, which will be discussed in the following.

The linear optical properties of our LNOI microdisk is then characterized at a low power level to avoid thermal and nonlinear effects. Using Laser1, we scan the transmission spectrum in a wide FW wavelength range (1520–1550 nm) using a very low input power of <100 μW, as shown in Fig. 3(a). Owing to a thin thickness, the microdisk mainly exhibits a single transverse electric (TE) mode family within the scanning range. We were unable to measure the transmission spectrum in the SH wavelengths. Because of a spare mode density, the order of each observed WGM can be identified according to numerical prediction. Typical resonance wavelengths of the 1st, 2rd, and 3rd radial orders of TE modes have been found by using a finite element mode solver (COMSOL). The simulated results fit the experimental data well, and each corresponding mode order is marked accordingly in the transmission spectrum. The indices ($q$, $m$) denote radial and azimuthal mode numbers, respectively. The modes of the same family have similar quality factors and transmission spectrum shapes. The resonator possesses a high loaded $Q$ factor of approximately $8.2 \times 10^5$ at ~1535 nm, the full width at half-maximum (FWHM) of which is approximately 1.87 pm, as shown in Fig. 3(b). It corresponds to the TE(1, 169) mode. The 1st radial TE mode has the largest effective refractive index and is used as the FW mode to excite SHG. The free spectral range (FSR) of the TE modes at the FW range is about 6.9 nm, which is in accordance with the measured FSR of 6.8 nm in the experiment. The calculated mode profiles of FW in the vicinity of 1535 nm are given in Figs. 3(c)–3(e), respectively. As can be seen from the figure,

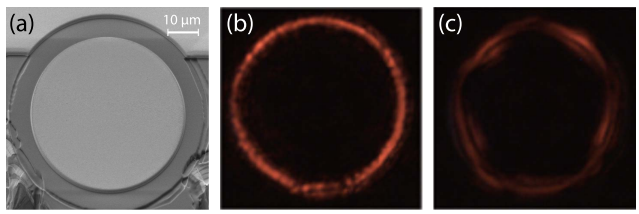


**Fig. 2.** Microscopy imaging of the fabricated LNOI microdisk. (a) SEM image of the LNOI microdisk before hydrofluoric acid etching. The diameter of the microdisk is 50 um. (b) Phase-matched SHG between fundamental FW and SH modes. (c) Slightly mismatched SHG between fundamental FW and higher-radial-order SH mode.

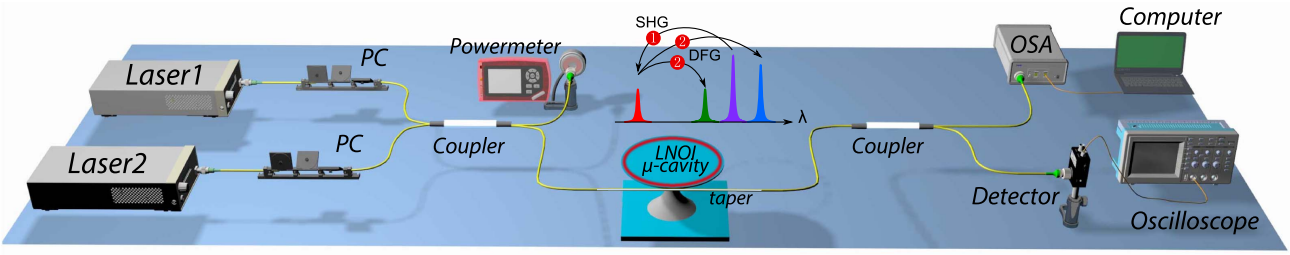


**Fig. 1.** Schematic illustration of the experimental setup for the cascading process in the LNOI microdisk. PC, polarization controller; coupler, 2 × 2 port fiber coupler; OSA, optical spectrum analyzer. Detector: InGaAs avalanche photodetector.

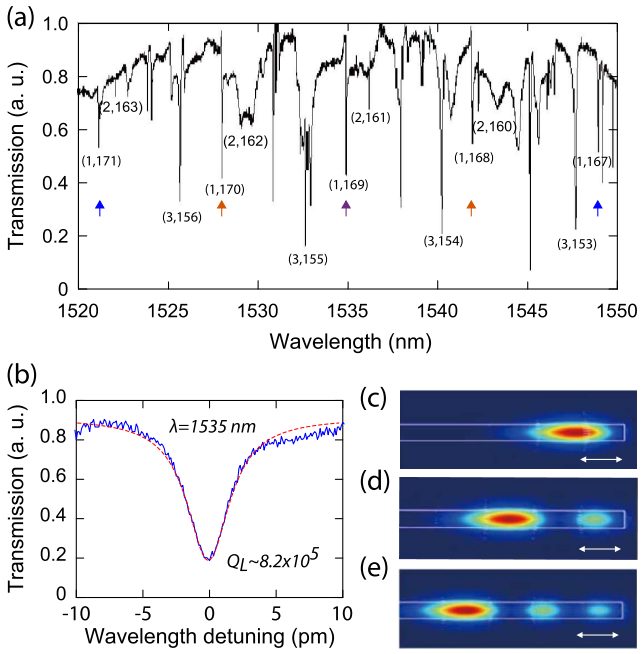


**Fig. 3.** Optical characterization of the LNOI microdisk. (a) Transmission spectrum of the microdisk at telecommunication wavelengths at low input power. The corresponding TE mode orders are marked. (b) A Lorentz fit of the measured FW resonance at ~1535 nm. (c)–(e) Calculated intensity profile of the corresponding 1st-, 2nd-, and 3rd-order radial TE modes at the FW wavelength. $n_{\text{eff}} = 1.65$, 1.58, and 1.51, respectively. The white arrows indicate the direction of the electric field.

the modes are well confined in the microdisk. Owing to the limitation of the thickness of the LN disk, transverse magnetic modes are seldom found at telecommunication wavelengths.

The first step in the cascading process is to generate efficient SHG. Injecting intense FW of 5 mW, we scan the FW wavelength (Laser1) to observe efficient SHG. The wavelength for efficient modal phase matching was found to be 1534.9 nm. When we tuned the pump into the resonance of TE(1, 169), efficient SHG via modal phase matching is observed. The bright scattered SH wave at NIR range seen from the optical microscope is shown in Fig. 2(b). Demonstration and analysis of SHG in LNOI microresonators can also refer to Ref. [20]. During the experiment, we also observed SHG in the case of a slightly phase mismatching condition at 1536.2 nm for TE(2, 161) mode, as shown in Fig. 2(c). Compared to Fig. 2(b), it is much darker, and periodic brightness and darkness can be observed along the rim of the LNOI microdisk, showing the backward and forward coupling of the FW and SH waves. As can be seen, the matching occurs between FW and higher-order radial SH modes. The pattern arises from the interference between mismatched orders of FW and SH modes mediated by quadratic nonlinearity [28], and the circumference of the LNOI microdisk corresponds to 10 times the coherent lengths in this case.

To demonstrate the cascading process, we locked the wavelength of FW to the resonance at 1534.9 nm to maintain the efficient SHG. We then added a signal light from Laser2 and scanned its wavelength to observed the DFG of the signal and the SH. The DFG process occurs when the signal is tuned at wavelengths of 1541.8 nm, corresponding to TE(1, 168), and 1548.9 nm, corresponding to TE(1, 167). The idler counterparts sit at 1528.0 nm, corresponding to TE(1,170), and 1521.2 nm, corresponding to TE(1,171), respectively. The spectra of the two experimental results are shown in Fig. 4 in orange and blue lines, respectively. The spectral resolution is set to be 0.1 nm. Considering that the third-order nonlinear coefficient of the LN crystal is small compared to the second-order one, the observed effective FWM process is a cascaded quadratic nonlinear processes, i.e., cSHGDFG. The direct Kerr effect in LNOI microcavities has only been recently demonstrated to obtain frequency comb generation using ultrahigh-$Q$ microring resonators at high input powers [29,30]; both parameters are much higher than this work. Comparing Fig. 4 to Fig. 3(a), we can see that FW, signal, and idle light are all 1st radial order TE modes, indicated by the arrows. In the experiment, when we tuned the signal light to other radial mode orders, we did not observe the idle light. The reason is that the modal phase matching condition and the mode overlapping are not satisfied at the same time, resulting in an extremely low efficiency.

Assuming zero detuning, phase matching, and undepleted pump conditions, we can adopt a simplified model to see the dependence relation. The cascading process resembles a subharmonic pumped optical parametric oscillation, and the amplitudes of SH and Idler waves have the form [11,31]

$$A_{\text{SH}} = \frac{\chi^{(2)}_{\text{eff}}\omega^2_{\text{SH}}}{k_{\text{SH}}c^2} A_P^2 L f(A_P, A_{\text{SH}}), \tag{1}$$

$$A_{\text{Idl}} = i\sqrt{\frac{n_{\text{Sig}}\omega_{\text{Idl}}}{n_{\text{Idl}}\omega_{\text{Sig}}}}\frac{A_{\text{SH}}}{|A_{\text{SH}}|} A^*_{\text{Sig}} \sinh(\kappa L) L f(A_{\text{SH}}, A_{\text{Sig}}, A_{\text{Idl}}), \tag{2}$$

$$\kappa^2 = \frac{\chi^{(2)}_{\text{eff}}\omega^2_{\text{SH}}\omega^2_{\text{Sig}}}{k_{\text{SH}}k_{\text{Sig}}c^4}|A_{\text{SH}}|^2. \tag{3}$$

Here, $A_j$ is the mode amplitude in the microresonator; $\omega_j$ is the optical angular frequency; $k_j$ is the wave vector; $\chi^{(2)}_{\text{eff}}$ is the effective nonlinear susceptibility; $f$ is the function of the modal overlap integral between mixing waves; $L$ is the light propagation distance in the microresonator; $n_j$ is the effective refractive index of the modes; $c$ is the speed of light in vacuum; and $j = P$, SH, Sig, and Idl represents pump, SH, signal, and idle, respectively.

The expected idle power from the cascading process is exponentially proportional to the SH (i.e., the square of FW).

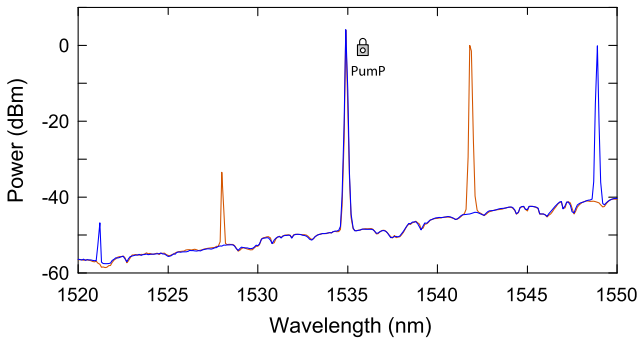


**Fig. 4.** Optical spectra of the cascading process with pumping fixed at 1534.9 nm and signal at 1541.8 nm (orange line) and 1548.9 nm (blue line).

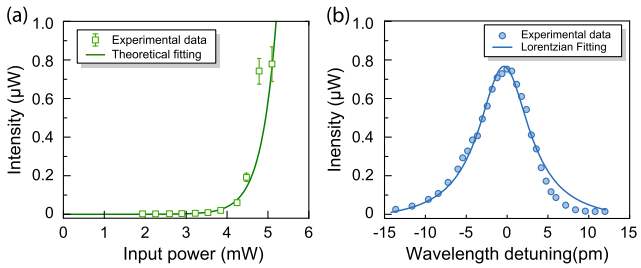


**Fig. 5.** Effective FWM process in the LNOI microdisk. (a) FW-idle power dependence and the theoretical fitting. The signal light intensity is maintained at 5 mW. (b) Idler intensity versus signal wavelength detuning and its Lorentz fit. The pump intensity is maintained at 5 mW.

To reconfirm this, we recorded the power of FW, signal, and idle light via the OSA spectrum. As shown in Fig. 5, the signal light intensity is maintained at 5 mW, while the pump power is increased from 0 to 5 mW. The intensity of the pump light is directly read by a power meter, and the energy of the idle light is measured by the OSA. The spectrum corresponds to the orange line in Fig. 4. During the experiment, the signal coupling is optimized by the polarization controller, and the photodetector is used to judge whether the system is stable. By varying the pump power, we obtained the power dependence of the generated idler. The energy dependence is shown in Fig. 5(a). The experimental data exhibit a sinh relation between the two as predicted by the theoretical modelling based on the cascaded quadratic nonlinear processes of cSHG/DFG. For simplicity, one can easily find that $P_{\mathrm{Idl}} \propto \sinh^2 P_P$ for the output light, with $P_{\mathrm{Idl}}$ and $P_P$ being the power of idle and pump, respectively. In the end, we can get a normalized conversion efficiency of approximately $10^{-4}$, equivalent to that reported in Ref. [22] where the direct DFG process was investigated. Although still at a low efficiency, the signal in this process is also amplified, that is optical parametric amplification is achieved. The effective large Kerr nonlinearity during the cascading process in the LNOI microresonators may be exploited for signal amplification or tunable wavelength conversion in telecommunication channels.

In addition, we also studied the relationship between idle and signal light by scanning the wavelength of the signal light, while keeping the pump light unchanged at 5 mW. As we know, with undepleted pump approximation, $P_{\mathrm{Idl}} \propto P_{\mathrm{Sig}}$. As shown in Fig. 5(b), the experimental data also satisfy a Lorentz linearity. The distortion of the result from the symmetric lineshape is due to the thermal effect [32]. Compared to Fig. 3(b), the Lorenz curve was slightly broadened with respect to a cold cavity. Higher pump and signal light energy results in higher conversion efficiency; however, coupling excessive energy into the microdisk for a long time may cause the microdisk to degrade or even crack in the $Q$ factor due to optical damage. The laser powers are therefore kept at moderate levels in our experiment. This problem can be mitigated by using higher-quality LNOI microresonators.

In summary, we have demonstrated an effective FWM in an on-chip LNOI microdisk resonator via cascading second-order nonlinear processes (cSHG/DFG). Our work makes promise for frequency conversion in integrated nonlinear photonics.

**Funding.** National Natural Science Foundation of China (NSFC) (11604206, 11734011, 61590934); National Key R&D Program of China (2018YFA0306301, 2017YFA0303701); Shanghai Municipal Education Commission (16CG08); Foundation for Development of Science and Technology of Shanghai (17JC1400400).

## REFERENCES

1. K. J. Vahala, Nature **424**, 839 (2003).
2. G. Lin, A. Coillet, and Y. K. Chembo, Adv. Opt. Photon. **9**, 828 (2017).
3. L. He, S. K. Ozdemir, and L. Yang, Laser Photon. Rev. **7**, 60 (2013).
4. M. R. Foreman, J. D. Swaim, and F. Vollmer, Adv. Opt. Photon. **7**, 168 (2015).
5. M. Aspelmeyer, T. J. Kippenberg, and F. Marquardt, Rev. Mod. Phys. **86**, 1391 (2014).
6. D. V. Strekalov, C. Marquardt, A. B. Matsko, H. G. L. Schwefel, and G. Leuchs, J. Opt. **18**, 123002 (2016).
7. J. U. Fürst, D. V. Strekalov, D. Elser, M. Lassen, U. L. Andersen, C. Marquardt, and G. Leuchs, Phys. Rev. Lett. **104**, 153901 (2010).
8. P. S. Kuo, J. Bravo-Abad, and G. S. Solomon, Nat. Commun. **5**, 3109 (2014).
9. A. W. Bruch, X. Liu, X. Guo, J. B. Surya, Z. Gong, L. Zhang, J. Wang, J. Yan, and H. X. Tang, Appl. Phys. Lett. **113**, 131102 (2018).
10. X. Zhang, Q.-T. Cao, Z. Wang, Y.-X. Liu, C.-W. Qiu, L. Yang, Q. Gong, and Y.-F. Xiao, Nat. Photonics **13**, 21 (2019).
11. J. S. Levy, M. A. Foster, A. L. Gaeta, and M. Lipson, Opt. Express **19**, 11415 (2011).
12. G. Poberaj, H. Hu, W. Sohler, and P. Günter, Laser Photon. Rev. **6**, 488 (2012).
13. A. Boes, B. Corcoran, L. Chang, J. Bowers, and A. Mitchell, Laser Photon. Rev. **12**, 1700256 (2018).
14. M. Zhang, C. Wang, R. Cheng, A. Shams-Ansari, and M. Lončar, Optica **4**, 1536 (2017).
15. R. Wu, J. Zhang, N. Yao, W. Fang, L. Qiao, Z. Chai, J. Lin, and Y. Cheng, Opt. Lett. **43**, 4116 (2018).
16. J. Lin, Y. Xu, Z. Fang, M. Wang, N. Wang, L. Qiao, W. Fang, and Y. Cheng, Sci. China Phys., Mech. Astron. **58**, 114209 (2015).
17. R. Wolf, Y. Jia, S. Bonaus, C. S. Werner, S. J. Herr, I. Breunig, K. Buse, and H. Zappe, Optica **5**, 872 (2018).
18. Z. Hao, J. Wang, S. Ma, W. Mao, F. Bo, F. Gao, G. Zhang, and J. Xu, Photon. Res. **5**, 623 (2017).
19. R. Luo, H. Jiang, S. Rogers, H. Liang, Y. He, and Q. Lin, Opt. Express **25**, 24531 (2017).
20. S. Liu, Y. Zheng, and X. Chen, Opt. Lett. **42**, 3626 (2017).
21. R. Wolf, I. Breunig, H. Zappe, and K. Buse, Opt. Express **25**, 29927 (2017).
22. R. Luo, Y. He, H. Liang, M. Li, J. Ling, and Q. Lin, "Optical parametric generation in a lithium niobate microring with modal phase matching," arXiv:1810.01299v1 (2018).
23. J. Moore, M. Tomes, T. Carmon, and M. Jarrahi, Opt. Express **19**, 24139 (2011).
24. M. Li, C.-L. Zou, C.-H. Dong, and D.-X. Dai, Opt. Express **26**, 27294 (2018).
25. V. Ulvila, C. R. Phillips, L. Halonen, and M. Vainio, Phys. Rev. A **92**, 033816 (2015).
26. J. Lin, Y. Xu, Z. Fang, M. Wang, J. Song, N. Wang, L. Qiao, W. Fang, and Y. Cheng, Sci. Rep. **5**, 8072 (2015).
27. Z. Fang, Y. Xu, M. Wang, L. Qiao, J. Lin, W. Fang, and Y. Cheng, Sci. Rep. **7**, 45610 (2017).
28. T. Carmon, H. G. L. Schwefel, L. Yang, M. Oxborrow, A. D. Stone, and K. J. Vahala, Phys. Rev. Lett. **100**, 103905 (2008).
29. C. Wang, M. Zhang, R. Zhu, H. Hu, H. Chen, and M. Lončar, in *Conference on Lasers and Electro-Optics* (2018), p. SW4M.3.
30. Y. He, Q.-F. Yang, J. Ling, R. Luo, H. Liang, M. Li, B. Shen, H. Wang, K. Vahala, and Q. Lin, "A self-starting bi-chromatic $LiNbO_3$ soliton microcomb," arXiv:1812.09610v1 (2018).
31. R. W. Boyd, *Nonlinear Optics*, 3rd ed. (Academic Press, 2008).
32. J. Wang, B. Zhu, Z. Hao, F. Bo, X. Wang, F. Gao, Y. Li, G. Zhang, and J. Xu, Opt. Express **24**, 21869 (2016).